Ain Shams Engineering Journal 9 (2018) 2767–2779

Contents lists available at ScienceDirect

Ain Shams Engineering Journal

journal homepage: www.sciencedirect.com

Electrical Engineering

Stability improvement of power systems connected with developed wind farms using SSSC controller

Ahmed Rashad [a], Salah Kamel [b], Francisco Jurado [c,*]

[a] Upper Egypt Electricity Distribution Company, Qena Rural Electrification Sector, Egypt
[b] Department of Electrical Engineering, Faculty of Engineering, Aswan University, 81542 Aswan, Egypt
[c] Department of Electrical Engineering, University of Jaén, 23700 EPS Linares, Jaén, Spain

ARTICLE INFO

Article history:
Received 8 November 2016
Revised 25 January 2017
Accepted 30 March 2017
Available online 7 November 2017

Keywords:
Combined wind farm
Double feed induction generator
Squirrel cage induction generator
FACTS
SSSC

ABSTRACT

This paper studies the performance of SCIG wind farm, DFIG wind farm, and a combined wind farm (CWF) during three-phase grid fault. The SCIG and DFIG wind farms are equipped with Static Synchronous Series Compensator (SSSC) whereas the combined wind farm did not have one. Since the CWF is composed of an equal number of Double Feed Induction Generators (DFIGs) and Squirrel Cage Induction Generators (SCIGs), it incorporated the main advantages of both types of generator. More specifically, the SCIG has a lower cost, but its drawback lies in its negative impact on system stability, especially when it operates without a shunt compensator. On the other hand, the DFIG, though more expensive, is better able to maintain the stability of the system. The SCIG and DFIG wind farms are equipped with SSSC controller to control the active and reactive line power flow. The results of a comparative study of DFIG and SCIG wind farms with SSSC and combined wind farm without SSSC during a three-phase grid fault showed that even though the SSSC improved the performance of the DFIG and SCIG wind farms, the CWF without the SSSC controller is found to have the best performance. The stability of the three wind farms is examined using Voltage Stability Index (VSI). All of the test scenarios are simulated with MATLAB.

1. Introduction

Since the middle of the 20th century, renewable energy sources have gained importance as an alternative to more conventional methods of electricity generation. Alternative energy sources have become a priority in Europe though the primary focus has been on wind energy. This is particularly the case in northern European countries, which have fewer hours of sunlight but no shortage of strong wind. This growing interest in wind energy has led to the construction of large wind farms. Not surprisingly, the rising amount of wind energy penetration has obliged power system operators to establish regulations regarding the connection of wind power plants to the grid.

Recent studies have targeted the impact of wind energy penetration on the electrical grid in steady state conditions and especially in emergency conditions. This impact is directly linked to the type of generator used to convert the stored energy from wind into electrical energy. Early wind farms were initially equipped with the Squirrel Cage Induction Generator (SCIG), and subsequently with the Doubly Fed Induction Generator (DFIG). Over the years, it was also found that the performance of an electrical grid with high wind energy penetration could be improved thanks to the installation of FACTS controllers.

The configuration and operational characteristics of wind farms has been the focus of much research in the literature. The enhancement of an SCIG wind farm with an SVC and STATCOM when wind speed and fault conditions vary is discussed in [1,2]. Similarly, other authors analyse the impact of a DFIG-based wind turbine on the grid at varying wind speeds and under different fault conditions [3–5]. Enhancement the performance of SCIG wind turbines using STATCOM during grid faults was discussed in [6–14]. A comparison between the ability of STATCOM and Static Var Compensators (SVC) to enhance the performance of SCIG wind farms was investigated in [15]. [16] used Other FACTS such as the thyristor controlled series capacitor (TCSC), series braking resistor (SBR) and, gate-controlled series capacitor (GCSC) were in order to

* Corresponding author.
E-mail addresses: ahmedrshadar@yahoo.com (A. Rashad), skamel@aswu.edu.eg (S. Kamel), fjurado@ujaen.es (F. Jurado).
Peer review under responsibility of Ain Shams University.

Production and hosting by Elsevier

https://doi.org/10.1016/j.asej.2017.03.015
2090-4479/

Nomenclature

p.u.	per-unit
AC	alternative current
DC	direct current
vds	direct component of stator voltage
vqs	quadratic component of stator voltage
ids	direct component of stator current
iqs	quadratic component of stator current
i′dr	direct component of rotor current with respect to stator
i′qr	quadratic component of rotor current with respect to stator
Lms	magnetizing inductance of stator
rs	stator resistance
Ls	self-inductance of stator
P	d/dt
ωr	rotor speed
r′r	rotor resistance with respect to stator
L′r	self-inductance of rotor with respect to stator
Θr	rotor angle
Crotor	rotor side converter
Cgrid	grid side converter
DFIG	doubly fed induction generator
SCIG	squirrel cage induction generator
CWF	combined wind farm
PCC	point of common connection
FACTS	flexible AC transmission system
SVC	static Var compensator
SSSC	static synchronous series compensator
STATCOM	static synchronous compensator
VSC	voltage source converter
PLL	phase-looked loop
Q	subscript refers to quadratic component of parameter
D	subscript refers to direct component of parameter
Pm	mechanical power
Tm	mechanical torque applied to the rotor
Tem	electrical torque
ωs	synchronous speed

improve stability of SCIG wind farm. Stability enhancement of DFIG wind farms using FACTS such as STATCOM or SVC were discussed in [17–25]. All of these studies conclude that DFIG-based wind farms equipped with FACTS devices have greater stability and operational reliability than SCIG-based wind farms also with FACTS devices. However, wind farms involve a significant financial investment, and in this sense, DFIG-based wind farms are even more expensive than other types.

The study described in this paper shows that wind farm performance can be significantly enhanced at no additional cost. This can be achieved with a Combined Wind Farm (CWF) consisting of an equal number of DFIGs and SCIGs without the use of any FACTS devices. The impact of wind speed variation on this kind of configuration is discussed in [26–28].

This research used the MATLAB Simulink computer application to model an SCIG wind farm equipped with a SSSC controller at a Point of Common Connection (PCC), a DFIG wind farm with a SSSC, and a CWF without a SSSC. The simulation results show the impact of a three-phase fault occurred at the PCC for these three types wind farms.

The rest of the paper is organized as follows. Section 2 describes the construction, modelling, and operation of an SCIG wind turbine, a DFIG wind turbine, and an SSSC. Section 3 provides the details of the test system used in this study. Section 4 presents the simulation results, and finally, Section 5 gives the conclusions that can be derived from this research.

2. Modelling of drive train

The next equation represents the power captured by rotor model of SCIG and DFIG wind turbines from the wind.

$$P_{cap} = \frac{1}{2}\rho\pi r^2 v^3 Cp(\beta,\lambda) \tag{1}$$

where P_{cap} is the power captured, ρ is the air density (nominally 1.22 kg/m^3), r is the radius of area swept by the turbine blades, v is the wind speed, and C_p is the coefficient performance of wind turbine. The power coefficient that is a function of the tip speed ratio λ and pitch angle β, Power coefficient of wind turbine C_p is given by the next equation [29]:

$$Cp = 0.5173\left(\frac{116}{\lambda i} - 0.4\beta - 5\right)e^{\frac{-0.0068}{\lambda i}} + 0.0086 \tag{2}$$

where,

$$\frac{1}{\lambda i} = \frac{1}{\lambda + 0.08\beta} - \frac{0.0035}{\beta^3 + 1} \tag{3}$$

β is the bitch angle of the blade in degree and λ is the tip speed ratio, it can be given by the following equation:

$$\lambda = \frac{\omega_r}{V} \tag{4}$$

where ω_r is the angular speed of the turbine. In practical designs, the maximum achievable C_p is below 0.5 for high speed, two blade wind turbines, and between 0.2 and 0.4 for slow speed turbines with more blades [6,29].

The next equations express the drive train model of SCIG and DFIG wind turbines.

$$T_{wt} - T_{mec} = 2H_r\frac{d\omega_r}{dt} \tag{5}$$

$$T_{wt} - T_e = 2H_g\frac{d\omega_g}{dt} \tag{6}$$

$$T_{mec} = T_e + 2H_g\frac{d\omega_g}{dt} + 2H_r\frac{d\omega_r}{dt} \tag{7}$$

where T_{wt} is the mechanical torque of wind turbine rotor shaft, ω_r is the angular speed of turbine, H_r is inertia of wind turbine rotor shaft, T_{mec} is the mechanical torque of generator shaft, T_e is the generator electrical torque, ω_g is the angular speed of generator, H_g is inertia of generator shaft [28,29].

Modelling SCIG, DFIG and SSSC.

The construction, modelling and operation of SCIG and DFIG wind turbines have been widely discussed in previous research such as [30,31].

2.1. SCIG wind turbine model

The SCIG belongs to the first generation of induction generators used in wind generation systems because of their low cost and easy maintenance. The SCIG can be classified as a fixed speed self-excited induction generator. Fig. 1 shows a single-line diagram of an SCIG wind turbine where the wind turbine rotor is coupled to the generator through a gear box while the stator is connected to the grid through a two-winding transformer. A capacitor bank is

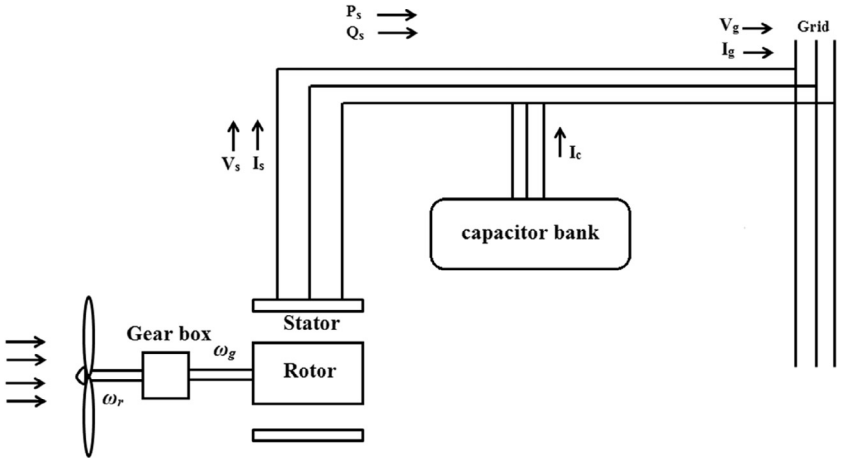

Fig. 1. Single-line diagram of the SCIG wind turbine.

connected across the stator terminals of a 3-phase induction generator in order to supply reactive power to the induction generator for the self-excitation process.

Eq. (1) is used to mathematically model the Squirrel Cage Induction Generator (SCIG) [31,32]:

$$\begin{bmatrix} v_{qs} \\ v_{ds} \\ 0 \\ 0 \end{bmatrix} = \begin{bmatrix} r_s + pL_s & 0 & pL_{ms} & 0 \\ 0 & r_s + pL_s & 0 & pL_{ms} \\ pL_{ms} & -\omega_r L_{ms} & r'_r + pL'_r & -\omega_r L'_r \\ \omega_r L_{ms} & pL_{ms} & \omega_r L'_r & r'_r + pL'_r \end{bmatrix} \begin{bmatrix} i_{qs} \\ i_{ds} \\ i'_{qr} \\ i'_{dr} \end{bmatrix} \tag{8}$$

The power extracted from the wind is limited by the stall effect or pitch angle control. This keeps the output power from exceeding its design limit. For this reason, the rotor is designed in such a way that its aerodynamic efficiency decreases as the wind speed increases in order to prevent the mechanical power extracted from the wind becoming too great. The output active and reactive power can be given as [32]:

$$P_s = \left(\frac{3}{2}\right)(V_{ds}I_{ds} + V_{qs}I_{qs}) \tag{9}$$

$$Q_s = \left(\frac{3}{2}\right)(V_{qs}I_{ds} - V_{ds}I_{qs}) \tag{10}$$

2.2. DFIG wind turbine model

The DFIG belongs to the second generation of induction generators used in wind generation systems. Eq. (11) is used to mathematically model the DFIG [31]:

$$\begin{bmatrix} v_{qs} \\ v_{ds} \\ v'_{qr} \\ v'_{dr} \end{bmatrix} = \begin{bmatrix} r_s + pL_s & 0 & pL_{ms}\cos\theta_r & -pL_{ms}\sin\theta_r \\ 0 & r_s + pL_s & pL_{ms}\sin\theta_r & pL_{ms}\cos\theta_r \\ pL_{ms}\cos\theta_r & pL_{ms}\sin\theta_r & r'_r + pL'_r & 0 \\ -pL_{ms}\sin\theta_r & pL_{ms}\sin\theta_r & 0 & r'_r + pL'_r \end{bmatrix} \begin{bmatrix} i_{qs} \\ i_{ds} \\ i'_{qr} \\ i'_{dr} \end{bmatrix} \tag{11}$$

However, the stator output and reactive power can be given by (9) and (10) while the rotor output and reactive power are given by (12) and (13) [30,33]:

$$P_r = \left(\frac{3}{2}\right)(V_{dr}I_{dr} + V_{qr}I_{qr}) \tag{12}$$

$$Q_r = \left(\frac{3}{2}\right)(V_{qr}I_{dr} - V_{dr}I_{qr}) \tag{13}$$

Fig. 2 shows a single line-diagram of DFIG wind turbine. The DFIG is connected to the grid with a three-winding transformer where the rotor is supplied from the third winding through a back-to-back voltage source converter. Output power is transferred from the stator to the grid through the other two windings of the three winding transformer. The DFIG can thus extract the maximum power from the wind turbine and regulate the reactive power transferred to the utility grid with the objective of controlling grid voltage regardless of the wind speed.

Fig. 2 shows that the rotor is connected to the AC/DC/AC converter, which is divided into two components: the rotor side converter C_{rotor} and the grid-side converter C_{grid}. The C_{rotor} and C_{grid} are Voltage-Sourced Converters that use forced-commutated power electronic devices (IGBTs) to synthesize an AC voltage from a DC voltage source. A capacitor connected on the DC side acts as the DC voltage source. A coupling inductor L is used to connect C_{grid} to the grid [34].

2.3. Power flow in DFIG

Fig. 2 illustrates the power flow of doubly fed induction generator connected to the grid. The mechanical power and the stator electrical power output are [34]:

$$P_m = T_m\omega_r \tag{14}$$

$$P_s = T_{em}\omega_s \tag{15}$$

For a loss less generator the mechanical equation is:

$$J\frac{d\omega_r}{dt} = T_m - T_{em} \tag{16}$$

In steady-state at fixed speed, $\frac{d\omega_r}{dt}$ is equal to zero so that the next equations can be concluded:

$$T_{em} = T_m \tag{17}$$

$$P_r = P_m - P_s \tag{18}$$

$$P_r = T_m\omega_r - T_{em}\omega_s \tag{19}$$

$$P_r = T_{em}(\omega_r - \omega_s) \tag{20}$$

$$P_r = -sP_s \tag{21}$$

$$s = \frac{\omega_s - \omega_r}{\omega_s} \tag{22}$$

Generally the absolute value of slip is much lower than 1 and consequently P_r is only a fraction of P_s. because ω_s is positive and constant for a constant frequency of grid voltage, the sign of P_r is a function of the slip sign (s). P_r is positive for negative slip

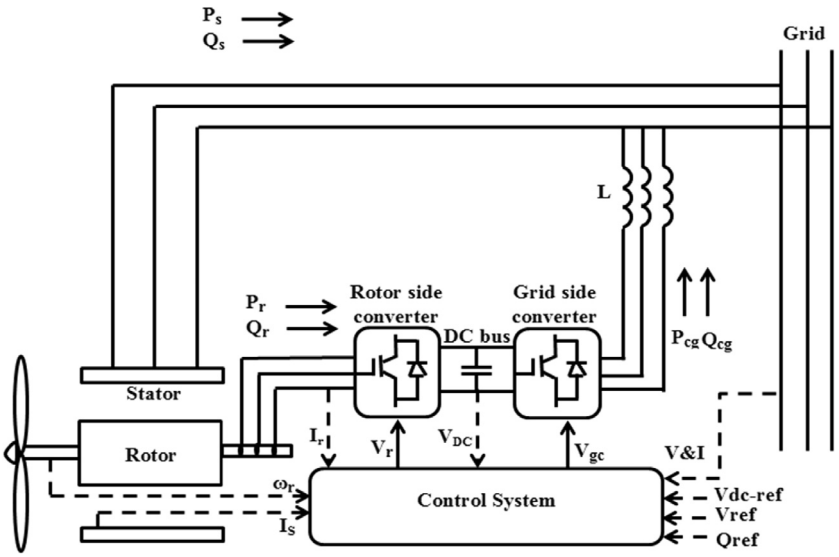

Fig. 2. Single line diagram of a DFIG wind turbine.

(super-synchronous speed) and it is negative for positive slip (sub-synchronous speed). For super-synchronous speed operation P_r is transmitted to DC bus capacitor and tends to raise the DC voltage. For sub-synchronous speed operation, P_r is taken out of DC bus capacitor and tends to decrease the DC voltage. C_{grid} is used to generate or absorb the power in order to keep the voltage at PCC within its allowable limits. This means that when the voltage at the PCC is lower than its allowable limits, the AC/DC/AC will inject a reactive power to regulate the voltage at PCC and when the voltage at the PCC is higher than its allowable limits, the AC/DC/AC will absorb a reactive power to regulate the voltage at PCC [34].

2.3.1. Rotor-side converter C_{rotor} control system

The power control loop of control system of C_{rotor} is illustrated in Fig. 3. C_{rotor} control system is used to control the rotor voltage (Vr) in order to control the ouput and reactive power at the grid terminal. Vdr and Vqr represent the direct and quadratic components of Vr. The output power is added to power losses then the total power is compared with the reference power obtained from tracking characteristic. The result is supplied to power regulator in order to generate Iqr-ref. Idr-ref which produced from comparing the grid voltage with the reference voltage and the error is reduced to zero by a current regulator (PI). Rotor current Ir is injected to VAR regulator to produce Idr and Iqr. Idr and Iqr are compared with Idr-ref and Iqr-ref respectively and the results are injected to VAR regulator to produce the rotor voltage Vr [34].

2.3.2. The grid-side converter C_{grid} control system

The grid-side converter is used to regulate the voltage of the DC bus capacitor. For the grid-side controller the d-axis of the rotating

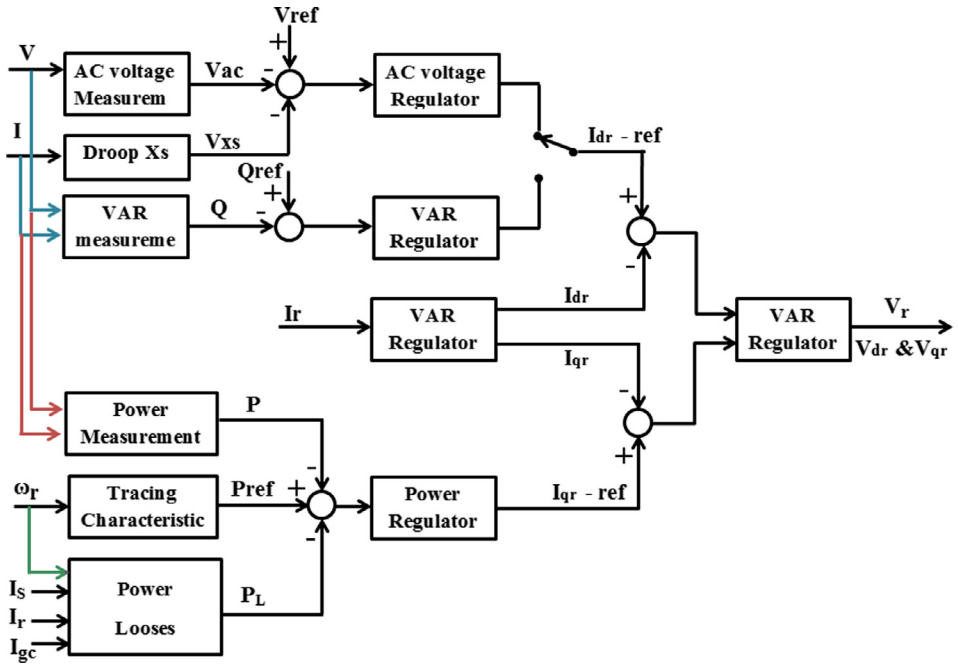

Fig. 3. Control system of C_{rotor}.

reference frame used for d-q transformation is aligned with the positive-sequence of grid voltage. The generic control loop is illustrated in Fig. 4 [34].

2.4. Static synchronous series compensator (SSSC)

The purpose of equipping grid-connected wind farm systems with Flexible AC Transmission System (FACTS) is to improve their stability. FACTS are a large family consisting of various devices, one of which is the SSSC. As its name implies, it is serially connected along with other FACTS devices, such as the STATCOM. The SSSC can operate either in a constant reactance mode (whether inductive or capacitive) or in a constant quadrature voltage mode. This paper focuses on the latter mode.

As can be observed in Fig. 5, the SSSC is a series-connection synchronous voltage sources that can vary the impedance of a transmission line by injecting voltage Vs in quadrature with the line current in order to improve stability at V_1. The value and phase of Vs is controlled by a Voltage Source Converter (VSC). The VSC uses a power electronic device to synthesize the Vs from the DC bus. The VSC is also gated by a controller [34].

Fig. 5. shows the connection of SSSC, it can be observed that SSSC is connected in series with transmission line between two voltages V_1 and V_2; SSSC injects voltage Vs in quadratic with line current in order to improve the stability of at V_1 [34].

$$V_s = V_2 - V_1 \tag{23}$$

Value and phase of Vs is controlled by using Voltage Source Converter (VSC). VSC uses a power electronic devise in order to synthesize Vs from the DC bus; also VSC is gated from a controller [34–37].

2.4.1. SSSC control system

Fig. 6 shows the SSSC control system. The control process can be illustrated as follows [37,38]:

1. The line current I is supplied to PLL in order to generate the phase angle Θ which is used to compute the direct and quadratic component of V1 and V2.
2. A measure system consists of three voltage measurements and one current measurement. Two of voltage measurements are used to generate V1q and V2q from V1 and V2 respectively and Θ while the third voltage measurement is used to generate Vdc from the voltage of DC voltage source (a capacitor in Fig. 5 acts as DC voltage source). The current measurement is used to generate I_d from I and Θ.
3. Vq is produced from comparing V1q and V2q. The Vq is compared with Vq-ref. Vq-ref and I_d are supplied to a voltage regulator in order to produce the quadratic component of converter voltage Vq-con.
4. The comparing output between Vdc with Vdc-ref is injected to DC voltage regulator to generate the direct component of converter voltage Vd-con.
5. Both Vq-con and Vd-con are injected with Θ to PWM to generate the plus of the voltage source converter VSC which will produce the converter voltage Vcon.
6. So that Vcon is is composed of two component Vq-con and Vd-con, since Vd-con ≅ 0 the Vs ≅ Vq-con which is always quadrature with the line current and its magnetite depend on difference between Vref and (V2-V1)
7. Vcon is transferred to the transmission line through a coupling transformer. The voltage that injected to the transmission line through a coupling transformer represents the voltage of SSSC (Vs).
8. Since Vs is equal to Vcon multiplied by the turn's ratio of coupling transformer, so that Vs ≅ Vq-con multiplied by the turn's ratio of coupling transformer which is always quadrature with the line current and its magnetite depend on difference between Vref and (V2-V1). If Vs is >0 SSSC is capacitive and injects a reactive power to the system while if Vs is <0 SSSC is inductive and absorbs a reactive power from the system.

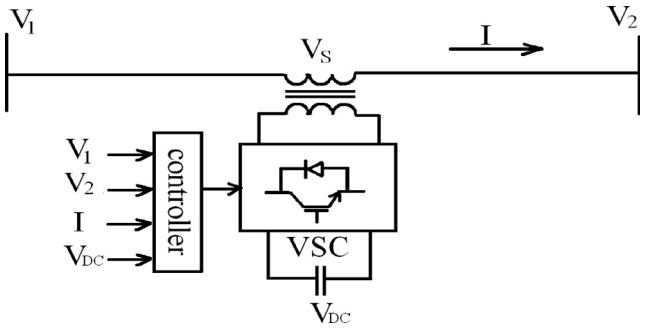

Fig. 5. Single-line diagram of an SSSC.

3. Voltage stability index

The Voltage Stability Indices are taken as an instrument that will measure the voltage stability of the studied power system [39]. The paper used a VSI formulation proposed in [40] order to that CWF without SSSC can give the same performance even better than wind farm based on DFIG wind turbines whatever it is associated with SSSC. The next equation represents principle of VSI used in this paper:

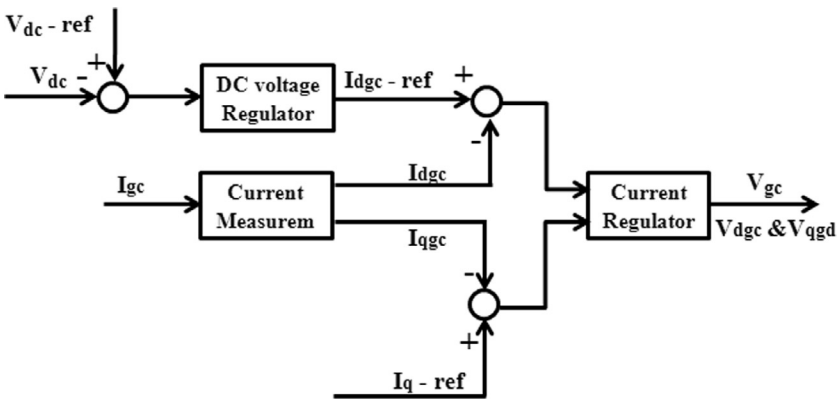

Fig. 4. Cgrid control system.

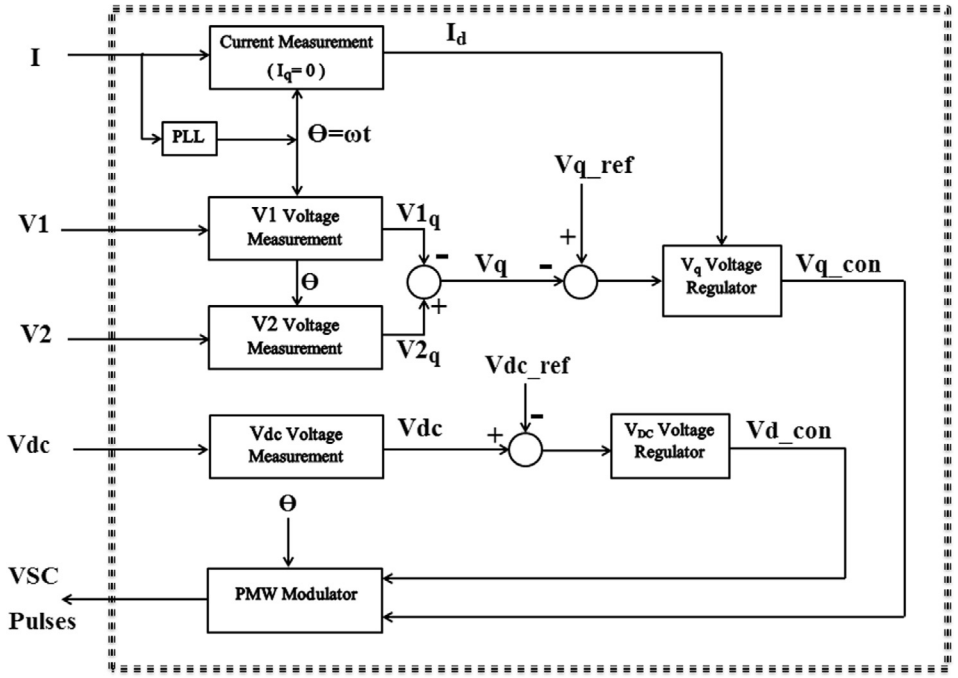

Fig. 6. SSSC control system.

$$VSI = \frac{|V_i|^2\sqrt{\left[\left(P_i - |I_i|^2R\right)^2 + \left(Q_i - |I_i|^2X\right)^2\right] + (R^2 + X^2)}}{2(P_iX - Q_iR)^2} - \frac{|V_i|^2\left(\left(P_i - |I_i|^2R\right)R + \left(Q_i - |I_i|^2X\right)X\right)}{2(P_iX - Q_iR)^2} \geqslant 1 \quad (24)$$

According to (24), VSI will have the following characteristics:

- When VSI is greater than 1, the transmission line is within its power transfer limit;
- When VSI is equal to 1, the transmission line is reaching maximum power transfer capability;
- When VSI is less than 1, maximum power transfer limit is violated and voltage becomes unstable.

4. Test system description

This paper studied three different of wind farms SCIG wind farm, DFIG wind farm and combined wind farm. Each wind farm consists of six 1.5 MW wind turbines to produce a 9-MW at 9 m/s wind speed and 575 v at bus B1. The wind farm is connected to a 25-kV distribution system exports power to a 120-kV grid through a 30-km, 25-kV feeder. The pitch angle control was applied to all wind turbines. Output power, reactive power and voltage were monitored at bus B1.

As shown in Fig. 7, the first wind farm in our study was an SCIG wind farm, in which all generators were SCIGs. Each wind turbine was connected to a 400 KVAR capacitor bank, and the wind farm was connected to an SSSC at bus B1.

Fig. 8 shows the second studied wind farm where all the wind farm generators are DFIGs, this wind farm is named as DFIG wind farm. The DFIG wind farm is connected to SSSC at bus B1.

Fig. 9 shows the combined wind farm (CWF), which comprised an equal number of SCIGs and DFIGs. Although the generators were not connected to an SSSC at bus B1, a 400 KVAR capacitor bank was connected to half of the SCIG wind turbines.

Table 1 shows the parameters of the SCIG wind turbine, DFIG wind turbine, and SSSC, transmission line and protection system which monitored the following: (i) Instantaneous AC over current; (ii) AC over current (positive sequence); (iii) AC current unbalance; (iv) AC undervoltage (positive sequence); (v) AC overvoltage (positive sequence); (vi) AC voltage unbalance (negative sequence); (vii) and AC voltage unbalance (zero sequence). All system parameters can be found in the SimPowerSystems demo file [18,22].

The power curves obtained for the SCIG and DFIG wind turbines are shown in Figs. 10 and 11, receptivity.

As can be observed in Figs. 10 and 11, working conditions were identical for both the SCIG and DFIG wind farms. In other words, the wind farms operated at the same wind speed to produce the same maximum power at the same base wind speed. As previously mentioned, the combined wind farm (CWF) was a combination of these same SCIG and DFIG wind turbines, which were used individually.

The strategy that had been followed in the reactive power injection during the grid fault was as follows:

1. In SCIG wind, farm the reactive power injection whatever during the grid fault or steady stat condition was depend on the operation of SSSC only.
2. In DFIG wind, farm the reactive power injection was depend on the operation of AC/DC/AC converter used in DFIG wind turbines and operation of SSSC together.
3. In combined wind farm the reactive power injection was depend on the operation of AC/DC/AC converter used in DFIG wind turbines only.

The ability of this the injected reactive power to regulate the voltage at PCC of studied wind farms with the grid was the main issues of this paper.

5. Simulation results

The performance of the three different wind farms (SCIG, DFIG and combined wind farms) under three phase fault condition is

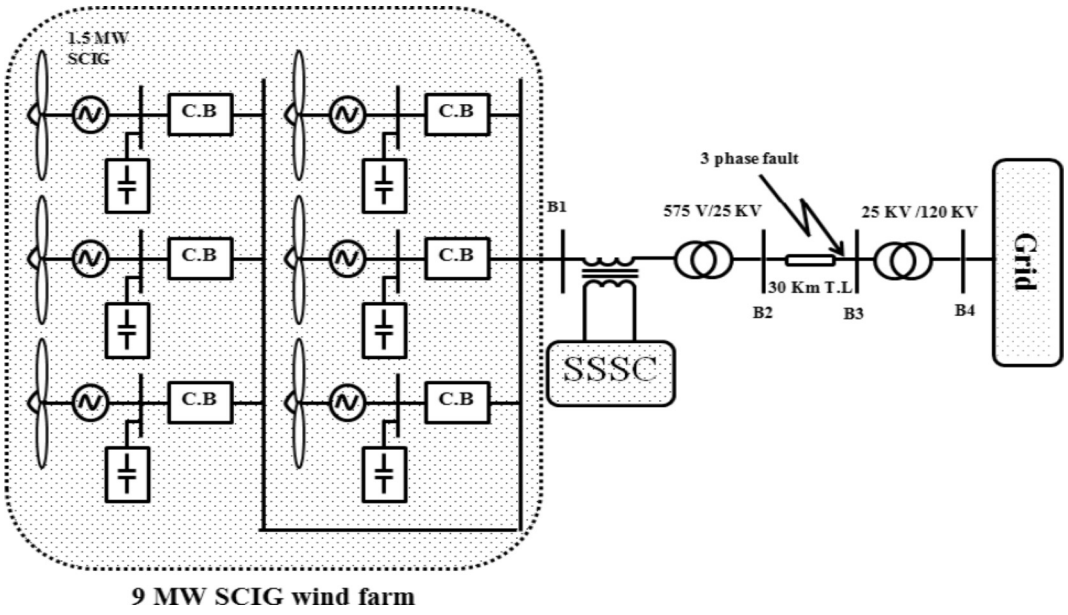

Fig. 7. Single-line diagram of the SCIG wind farm.

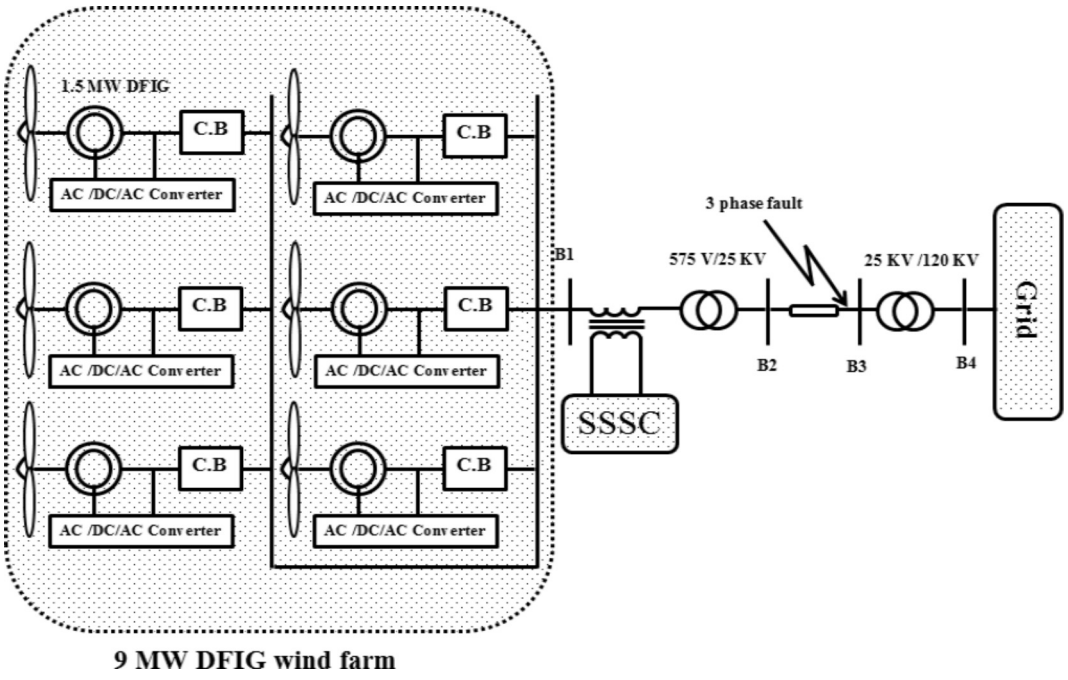

Fig. 8. Single line of studied DFIG wind farm.

studied. The three phase fault occurred at time equals to 16 s of the simulation time and continued for period equals to 0.500 s. The comparison is investigated among the combined wind farm without SSSC controller, SCIG wind farms occupied with SSSC and DFIG wind farm with and without SSSC under three phase fault condition.

5.1. Impact of a three-phase fault on the output power (P) of the three wind farms

As shown in Fig. 12, the output power (P) of the SCIG wind farm dropped to zero p.u. and remained at zero until the end of the simulation time. This means that the SCIG wind farm was disconnected from the grid and was unable to reconnect until after fault clearance. In contrast, the CWF and DFIG with and without SSSC were still able to remain connected to the grid despite the fact that their output power (P) experienced a sharp decrease. Also it can be observed that output power (P) of DFIG wind farm with SSSC is oscillated between 16.23 and 0 MW.

Table 2 shows the values of P of the three wind farms at different times. As can be observed from Table 2 and Fig. 12, the performance of CWF during fault period is much better than DFIG wind farm whatever it is occupied with or without SSSC except DFIG wind farm reached its steady state faster than CWF. CWF reached to its steady state gradually whereas DFIG wind farm suffers from sharp increase and decrease before reaching to the

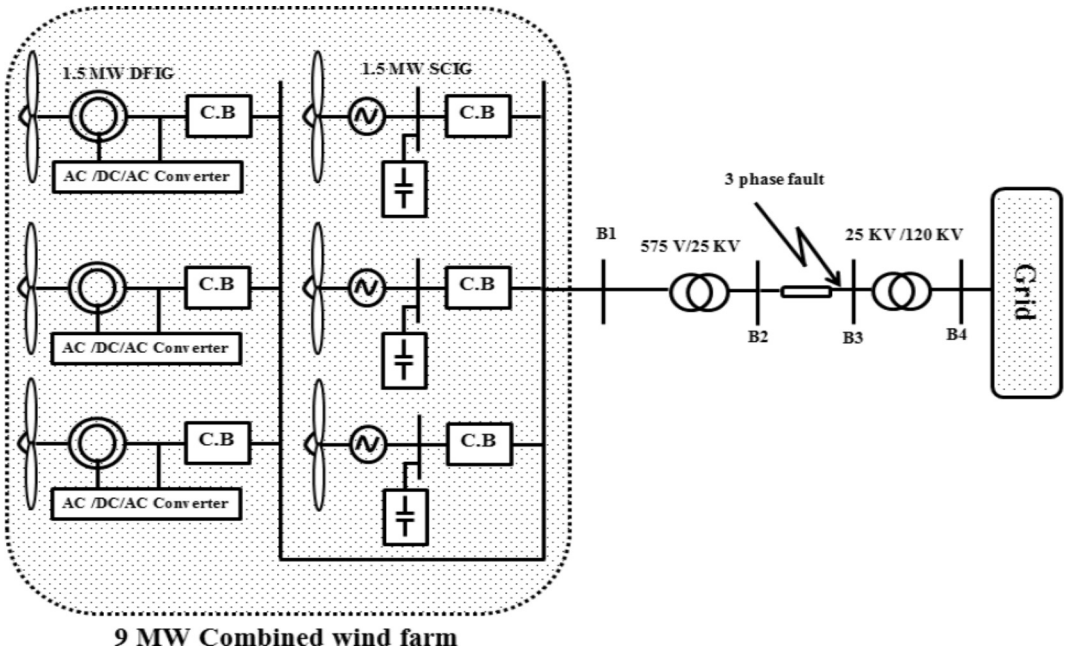

Fig. 9. Single line of studied combined wind farm.

Table 1
Test system parameters.

Parameter	Value	Unit
(a) SCIG wind turbine		
Maximum power at based wind speed	1.5	MW
Based wind speed	9	m/s
Operating wind speed	8	m/s
(b) DFIG wind turbine		
Maximum power at based wind speed	1.5	MW
Based wind speed	9	m/s
Operating wind speed	8	m/s
(c) Transmission line		
Positive-sequence resistances	0.1153	Ω/km
Positive-sequence inductances	1.05 e^{-3}	H/km
Positive-sequence capacitances	11.33 e^{-9}	F/km
Length of transmission line	30	km
(d) SSSC used in case studied		
Rating of SSSC	3	MVA
Nominal line voltage	575 * 1.73	v
DC link normal voltage	1200	v
DC link total equivalent capacitance	100 e^{-6}	F
(e) AC/DC/AC converter		
Rating of AC/DC/AC converter	0.83	MVAR
DC link normal voltage	1200	v
DC link total equivalent capacitance	20 e^{-3}	F

Parameter	Minimum value (pu)	Maximum value (pu)	Delay time (sec)
(f) AC voltage, rotor speed and current protection			
AC under/over voltage for SCIG	0.85	1.1	0.15
Under/over rotor speed for SCIG	1	1.05	5
Maximum AC current unbalance for SCIG	0.4		0.2
Maximum AC current for SCIG	1.1		
AC under/over voltage for DFIG	0.85	1.1	0.1
Under/over rotor speed for DFIG	0.3	1.5	5
Maximum AC current unbalance for DFIG	0.4		0.2
Maximum AC current for DFIG	1.1		

steady state. In steady stat condition it can be observed that the CWF can give the same performance of the other two wind farms associated with SSSC. The performance of CWF is much better than the performance of other two wind farms during fault condition.

5.2. Impact of a three-phase fault on the voltage (V) of the three wind farms

As can be observed in Fig. 13 and Table 3, the SCIG wind farm suffers from sharp decrease in voltage at PCC consequently with

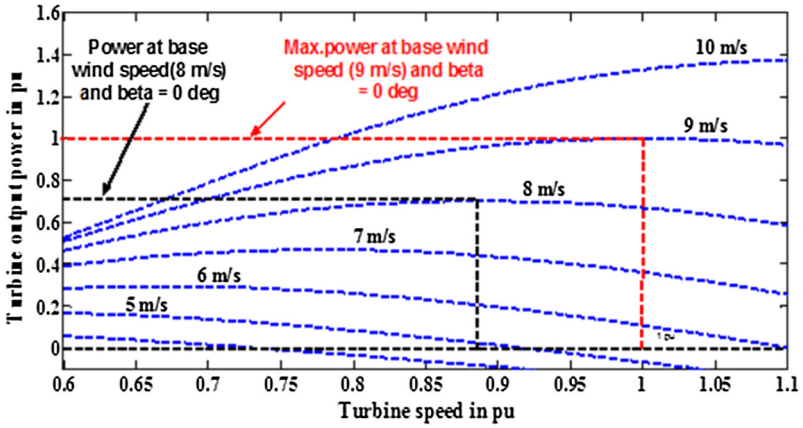

Fig. 10. SCIG turbine power characteristic.

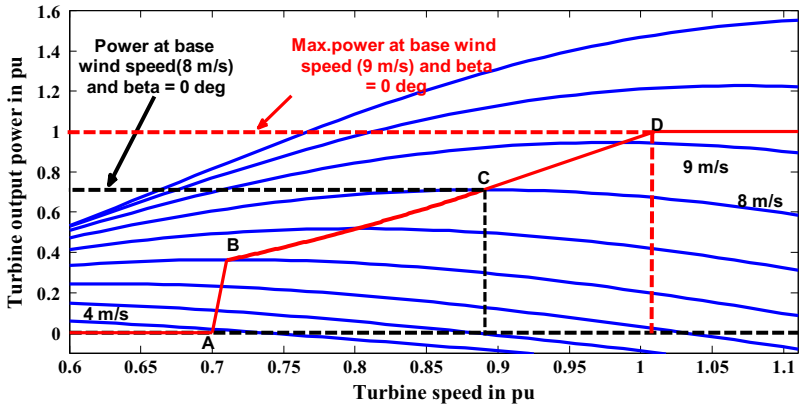

Fig. 11. DFIG turbine power characteristic.

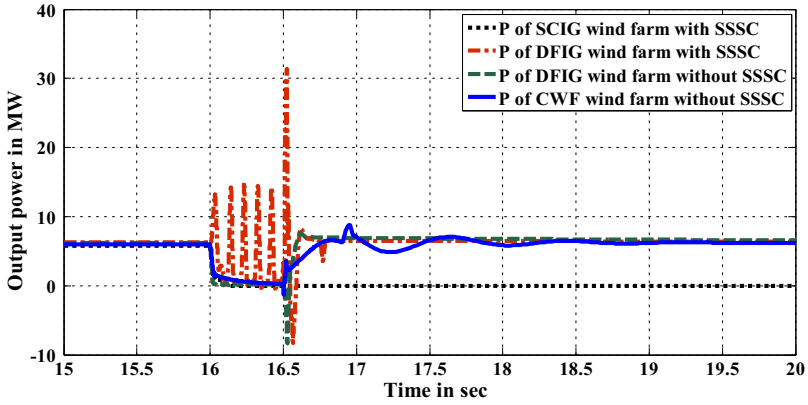

Fig. 12. Impact of three phase fault on output power (P) of the three wind farms.

Table 2
Output power (MW) of the three wind farms during different times of fault.

Wind farm	Fault occurrence at 16.03 s	Fault clearance at 16.49 s	Fault clearance at 16.550 s
SCIG wind farm with SSSC	1.080	0	0
DFIG wind farm with SSSC	13.03	0.65	15.7
DFIG wind farm without SSSC	0.32	0.29	1.03
Combined wind farm without SSSC	1.618	0.26	3.54

the fault occurrence till it reached to 0 p.u before fault clearance. Hence, protection system disconnects the SCIG wind farm from the grid to keep the system stability. This action explains the dropping down of output power of SCIG wind farm to zero till the end of simulation.

Also, it can be observed that the CWF voltage at PCC during the fault period is greater than the voltage of DFIG wind farm without SSSC while the voltage of DFIG wind farm with SSSC is oscillated between 0.5 pu and pu 2.16. Fig. 14 and Table 4 show the VSI of three wind farms during the simulation time.

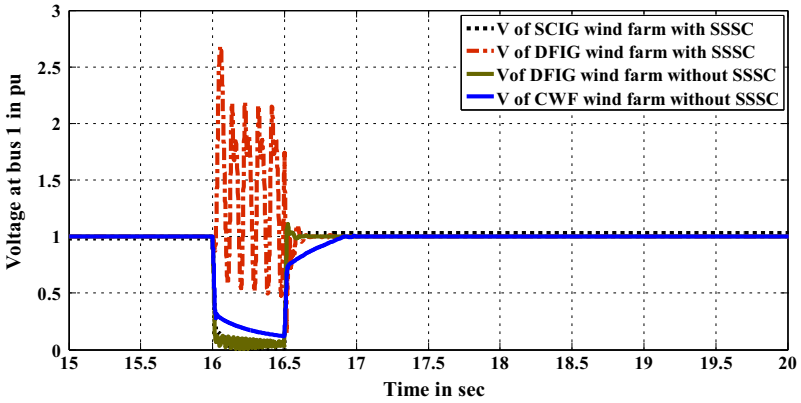

Fig. 13. The voltage at bus 1 of the three wind farms.

Table 3
Impact of three phase fault on voltage (p.u) of the three wind farms.

Wind farm	Fault occurrence at 16.03 s	Fault clearance at 16.49 s	Fault clearance at 16.55 s
SCIG wind farm with SSSC	0.17	0	1.04
DFIG wind farm with SSSC	1.3	1.2	0.95
DFIG wind farm without SSSC	0.11	0.05	1.03
Combined wind farm without SSSC	0.29	0.12	0.78

Table 4
Values of VSI during different times of fault.

Wind farm	Fault occurrence at 16.03 s	Fault clearance at 16.49 s	Fault clearance at 16.55 s
SCIG wind farm with SSSC	VSI < 1	VSI < 1	VSI > 1
DFIG wind farm with SSSC	VSI < 1	VSI < 1	VSI > 1
DFIG wind farm without SSSC	VSI < 1	VSI < 1	VSI > 1
Combined wind farm without SSSC	VSI < 1	VSI < 1	VS I > 1

From Fig. 14 and Table 4 it can be observed that the impact of performance of CWF during the fault on voltage stability of interconnected grid is much better performance than SCIG wind farm associated with SSSC and the same impact of performance of DFIG wind farm associated with or without SSSC but CWF is much lower cost than DFIG wind farm.

5.3. Impact of the three-phase fault on the reactive power (Q) of the three wind farms

From Fig. 15 and Table 5, it can be observed that the injected reactive power at the PCC in case of CWF without SSSC is much higher than the injected reactive power of DFIG wind farm without SSSC and SCIG wind farm with SSSC during whole period of fault. Also, it can be noted that the injected reactive power in case of CWF came from to the operation of AC/DC/AC converter of DFIG. The injected reactive power in case of DFIG wind farm with SSSC was due to the operation of AC/DC/AC converter and the operation of SSSC while the injected reactive power of SCIG wind farm is mainly based on the operation of SSSC. The injected reactive power in case of combined wind farm was used to regulate the voltage at the PCC and compensate the reactive power demanded by the SCIG used in combined wind farm. The output and reactive power of individual SCIG and DFIG wind turbines used in CWF are shown in Figs. 16 and 17.

From Fig. 16 it can be observed that during fault the output power of DFIG wind turbines was dropped to zero while SCIG wind turbines is still work and produce power so that the outcome of CWF will not be zero during the fault period and this explained the output power curve of CWF during fault shown in Fig. 12.

Fig. 17 shows that during fault period the reactive power is negative which means that the injected reactive power is used to regulate the voltage at PCC and hence keep connection of CWF to the grid. After fault clearance the reactive power of SCIG wind turbines is positive while the reactive power of DFIG wind turbines is negative which mean the injected reactive power by AC/DC/AC con-

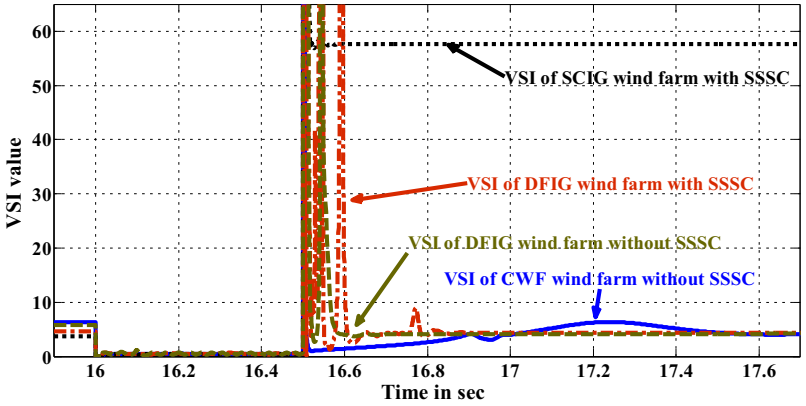

Fig. 14. The VSI of the three wind farms.

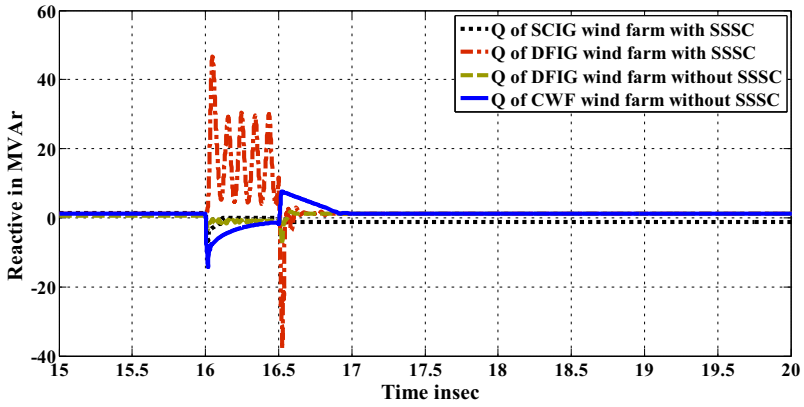

Fig. 15. The absorbed reactive power at bus 1 of the three wind farms.

Table 5
Values of reactive power in MVAr during different times of fault.

Wind farm	Fault occurrence at 16.03 s	Fault clearance at 16.49 s	Fault clearance at 16.55 s
SCIG wind farm with SSSC	−6.01	−0.008	−1.31
DFIG wind farm with SSSC	Oscillate 30.17 and 5.22	−37.13	−1.55
DFIG wind farm without SSSC	−1.7	−0.9	−0.54
Combined wind farm without SSSC	−14.13	−1.32	4.20

verter is used to compensate the demanded reactive power of SCIG wind turbines. This explained the reactive power curve of CWF during fault shown in Fig. 15.

The disturbance in voltage of DFIG wind farm with SSSC at PCC during the fault period was due to the disturbance on reactive power at PCC during the fault period as shown in Fig. 15. This disturbance can be explained by mentoring the voltage of DC (Vdc) bus of SSSC and the voltage of DC (Vdc) bus of AC/DC/AC converter of DFIG. Fig. 18 shows the Vdc of DFIG converters of DFIG wind with and without SSSC. Also Fig. 18 shows the Vdc of SSSC in cases of DFIG wind farm with SSSC.

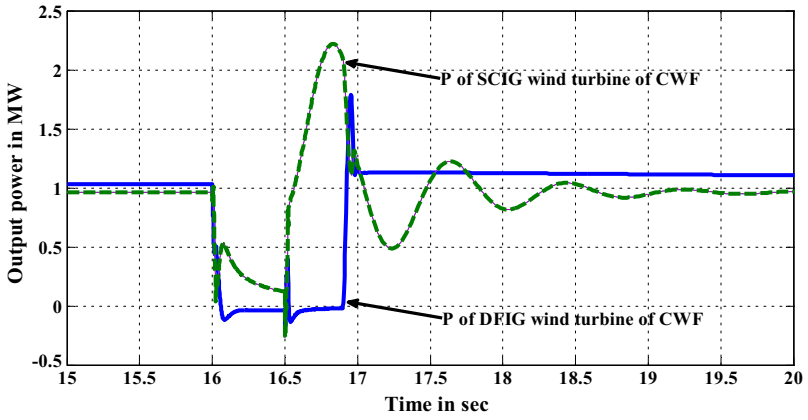

Fig. 16. Output power of SCIG and DFIG wind turbine used in CWF.

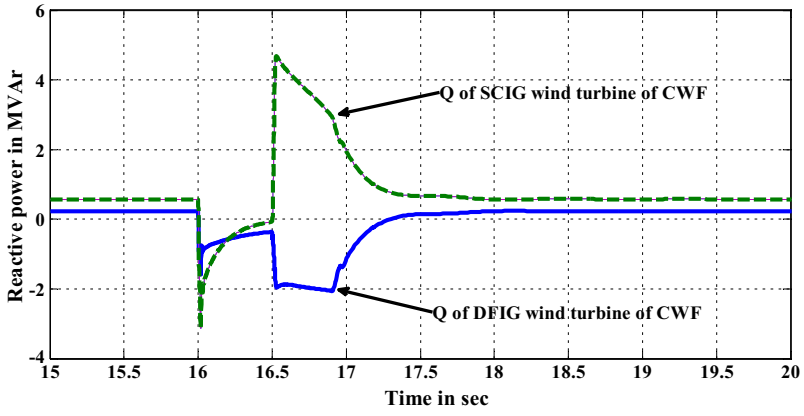

Fig. 17. Absorbed reactive power of SCIG and DFIG wind turbine used in CWF.

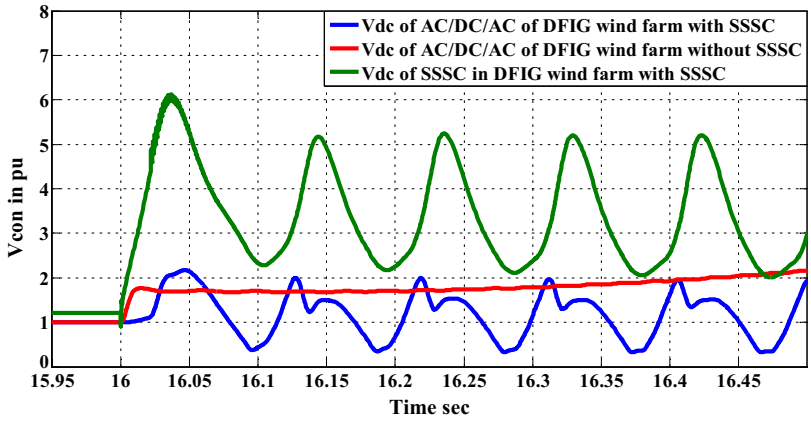

Fig. 18. Vdc of SSSC and Vdc of DFIG converters.

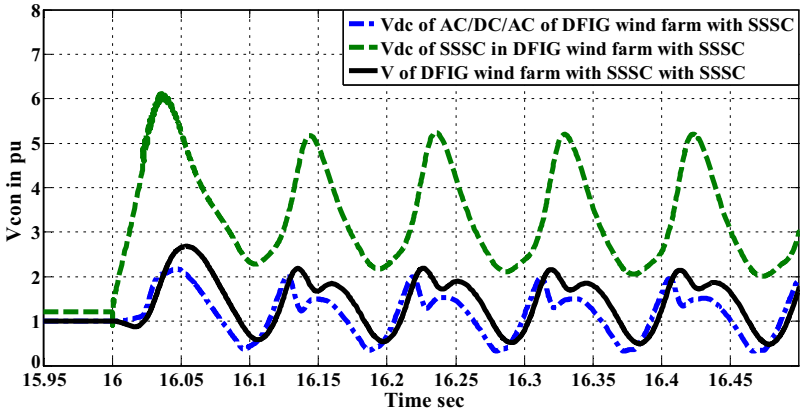

Fig. 19. Impact of overlap between Vdc of SSSC and Vdcod DFIG conveters on V of DFIG wind farm with SSSC at PCC.

From Fig. 18, it can be observed that in case of DFIG wind farm with SSSC there was Proportionality or synchronization between Vdc of SSSC and Vdc of DFIG converters during fault period which means that there was an overlap between the operation of SSSC and DFIG converters. This overlap will affect on the voltage of DFIG wind farm at PCC as shown in Fig. 19. Fig. 19 shows the impact of overlap between Vdc of SSSC and Vdc of DFIG converters on V of DFIG wind farm with SSSC at PCC

6. Conclusions

This study compared the performance of three types of wind farm during a three-phase fault. The wind farms analysed were the following: (i) a SCIG wind farm equipped with an SSSC controller; (ii) a DFIG wind farm based equipped with and without SSSC; (iii) a combined wind farm (CWF) without any controller. During the fault, the SCIG wind farm with SSSC with a rating of 3 MVAR (equal to one third of the wind farm rating) was disconnected from the grid due to under voltage. The DFIG with and without SSSC and the CWF without SSSC remained connected to the grid but the output power of the CWF was found to be higher than that of the DFIG wind farm during the fault.

Furthermore, the voltage of the DFIG wind farm with SSSC experienced a significant disturbance during the fault period. This disturbance was due to the extreme oscillation of the injected reactive power at the PCC of the DFIG wind farm, coming from the SSSC. In contrast, this was not the case in the CWF because it had no SSSC. The results obtained in this study indicate that the CWF is a reliable wind generation system because it does not require a controller to maintain system stability during a fault condition. This signifies that this type of CWF has lower installation costs and thus is more cost-effective than other types of wind farm.

References

[1] Noureldeen, Rihan M, Hasanin. Stability improvement of fixed speed induction generator wind farm using STATCOM during different fault locations and durations. Ain Shams Eng J 2011;2(1):1–10.
[2] Gounder YK, Nanjundappan D, Boominathan V. Enhancement of transient stability of distribution system with SCIG and DFIG based wind farms using STATCOM. IET Renew Power Gener 2016;10(8):1171–80.
[3] Gautam D, Vittal V, Harbour T. Impact of increased penetration of DFIG-based wind turbine generators on transient and small signal stability of power systems. IEEE Trans Power Syst 2009;24(3):1426–34.
[4] Rashad A, Noureldeen O. Modeling and investigation of Gulf El-Zayt wind farm for stability studying during extreme gust wind occurrence. Ain Shams Eng J 2014;5:137–48.
[5] Fernandez LM, Jurado F, Saenz JR. Aggregated dynamic model for wind farms with doubly fed induction generator wind turbines. Renewable Energy 2008;33(1):129–40.
[6] Ledesma P, Usaola J, Rodriguez J. Transient stability of a fixed speed wind farm. Renewable Energy 2003;28:1341–55.
[7] Ahsan S, Siddiqui A. Dynamic compensation of real and reactive power in wind farms using STATCOM. Perspect Sci 2016;8:519–21.
[8] Hossain MJ, Pota H, Ramos R. Robust STATCOM control for the stabilisation of fixed-speed wind turbines during low voltages. Renewable Energy 2011;36:2897–905.
[9] Ramirez D, Martinez S, Blazquez F, Carrero C. Use of STATCOM in wind farms with fixed-speed generators for grid code compliance. Renewable Energy 2012;37:202–12.
[10] Laouer M, Mekkaoui A, Younes M. STATCOM and Capacitor Banks in a fixed-speed wind farm. Energy Proc 2014;50:882–92.

[11] Heydari-doostabad H, Khalghani MR, Khooban MH. A novel control system design to improve LVRT capability of fixed speed wind turbines using STATCOM in presence of voltage fault. Int J Electr Power Energy Syst 2016;77:280–6.
[12] Boubekeur B, Gherbi A, Mellah H. Application of STATCOM to increase transient stability of wind farm. Am J Electr Power Energy Syst 2013;2:50–6.
[13] Wessels C, Hoffmann N, Molinas M, Fuchs FW. StatCom control at wind farms with fixed-speed induction generators under asymmetrical grid faults. IEEE Trans Industr Electron 2013;60:2864–73.
[14] Pereira R, Ferreira C, Barbosa F. Comparative study of STATCOM and SVC performance on dynamic voltage collapse of an electric power system with wind generation. IEEE Latin Am Trans 2014;12:138–45.
[15] Mohammadpour HA, Ghaderi A, Mohammadpour H, Ali MH. Low voltage ride-through enhancement of fixed-speed wind farms using series FACTS controllers. Sustain Energy Technol Assess 2015;9:12–21.
[16] Ananth D, Kumar GN. Fault ride-through enhancement using an enhanced field oriented control technique for converters of grid connected DFIG and STATCOM for different types of faults. ISA Trans 2016;62:2–18.
[17] Ananth DVN, Nagesh Kumar GV. Mitigation of voltage dip and power system oscillations damping using dual STATCOM for grid connected DFIG. Ain Shams Eng J 2017;8(4):581–92.
[18] Masaud T, Sen PK. A comparative study of the implementation of STATCOM and SVC on DFIG-based wind farm connected to a power system. IEEE power energy society general meeting 2012:1.
[19] Abobkr AH, El-Hawary M. Fault ride-through capability of doubly-fed induction generators based wind turbines. Electrical power and energy conference (EPEC); 2015. p. 8–15.
[20] Wang L, Truong D-N. Stability enhancement of DFIG-based offshore wind farm fed to a multi-machine system using a STATCOM. IEEE Trans Power Syst 2013;28:2882–9.
[21] Masaud TM, Sen P. Study of the implementation of STATCOM on DFIG-based wind farm connected to a power system. IEEE PES innovative smart grid technologies (ISGT); 2012. p. 1–7.
[22] Garg A, Singh RP. Dynamic performance analysis of IG based wind farm with STATCOM and SVC in MATLAB/SIMULINK. Int J Comput Appl 2013;71(23).
[23] Fernandez LM, Garcia CA, Jurado F. Comparative study on the performance of control systems for doubly fed induction generator (DFIG) wind turbines operating with power regulation. Energy 2008;33(9):1438–52.
[24] Ananth DVN, Kumar GVN. Fault ride-through enhancement using an enhanced field oriented control technique for converters of grid connected DFIG and STATCOM for different types of faults. ISA Transactions 2016;62:2–18.
[25] Rashad A, Noureldeen O, Abdelwahab MA. Operation of hybrid wind farm based on SCIG and DFIG under gust wind speed. J Eng Sci Assiut Univ 2011;39 (3):637–48.
[26] Li H, Yang C, Zhao B, Wang HS, Chen Z. Aggregated models and transient performances of a mixed wind farm with different wind turbine generator systems. Electric Power Syst Res 2012;92:1–10.
[27] Rashad A, Noureldeen O, Abdelwahab MA. Behavior of mixed wind farm based on SCIG and DFIG during wind gust occurrence. 15th International middle east power systems conference. Egypt: Alexandria University 2012;23–25:1–8.
[28] Fernandez LM, García CA, Saenz JR, Jurado F. Equivalent models of wind farms by using aggregated wind turbines and equivalent winds. Energy Convers Manage 2009;50(3):691–704.
[29] Heier S. Grid integration of wind energy conversion systems. Chicester: John Wiley & Sons; 1998.
[30] Movahednasab A, Madani SM, Shahbazi MM. Modeling of a squirrel cage induction generator IEEE Electrical Machines and Systems International Conference 2008:4267–71.
[31] Li S, Haskew TA, Williams KA, Swatloski RP. Control of DFIG wind turbine with direct-current vector control configuration. IEEE Trans Sustain Energy 2004;3 (1):1–11.
[32] Simões MG, Farret FA. Renewable energy systems: design and analysis with induction generators. CRC Press; 2004.
[33] Krause PC, Wasynczuk O, Sudhoff SD. Analysis of electric machinery and drive systems. 2nd ed. IEEE; 2002.
[34] Wind Turbine Induction Generator, Matlab/Simulink Help, SimPower-Systems Blocks.
[35] Sen KK. SSSC-static synchronous series compensator: theory, modeling, and applications. IEEE Trans Power Deliv 1998;13(1):241–6.
[36] Jowder FAL. Influence of mode of operation of the SSSC on the small disturbance and transient stability of a radial power system. IEEE Trans Power Syst 2005;20(2):935–42.
[37] Kamel S, Jurado F, Chen Z. Power flow control for transmission networks with implicit modeling of static synchronous series compensator. Int J Electr Power Energy Syst 2015;64:911–20.
[38] MATLAB/Simulink Documentation, Available <http://www.mathworks.com>.
[39] Vittal E, O'Malley M, Keane A. A steady-state voltage stability analysis of power systems with high penetrations of wind. IEEE Trans Power Syst 2010;25:433–42.
[40] Zheng C, Kezunovic M. Distribution system voltage stability analysis with wind farms integration North American power symposium (NAPS); 2010. p. 1–6.